Research Article Vol. 4, No. 12 / 15 Dec 2021 / OSA Continuum 3176
OSA CONTINUUM

Acousto-optic modulator pulse-shaper compression of octave-spanning pulses from a stretched hollow-core fiber

ANTHONY CATANESE,* BRIAN KAUFMAN, CHUAN CHENG, ERIC JONES, MARTIN G. COHEN, AND THOMAS WEINACHT

Department of Physics and Astronomy, Stony Brook University, Stony Brook, New York 11790, USA
*anthony.catanese@stonybrook.edu

Abstract: We demonstrate spectral broadening and compression of amplified pulses from a titanium sapphire laser system using an argon-filled stretched, hollow-core fiber and an acousto-optic modulator based pulse-shaper. We characterize the pulses using pulse-shaper assisted collinear frequency resolved optical gating, pulse-shaper assisted D-scans, and D-scans using a variable path length water cell. The different compression and characterization approaches consistently compress the pulses down to < 6 fs, less than ~1 fs from the transform limit. We discuss prospects for pulse shape spectroscopy with these broadband pulses, given our control over the spectral amplitude and phase.

1. Introduction

Amplified, few-optical-cycle pulses play a key role in strong field science and time resolved measurements. They are instrumental in strong field ionization and high harmonic generation, and serve as a cornerstone of attosecond science [1]. Amplified Ti:Sapphire lasers are generally limited to pulse durations greater than ~ 20 fs, and therefore post amplification spectral broadening and pulse compression are typically employed to reduce pulse duration.

Self-phase modulation in hollow core fibers (HCF) is a straightforward mechanism that has been employed to broaden the bandwidth of amplified laser systems, allowing for pulse compression down to 10 fs [2]. A limiting aspect of HCFs is poor transmission of the fiber for lengths of 1m or greater due to sagging of the fiber and grazing incidence losses [3]. These losses can be mitigated by stretching the fiber. Thus, stretched hollow-core fibers (S-HCF) are rapidly advancing the technology to generate octave-spanning bandwidths, which when compressed, can support <5 fs pulses [4]. The source of spectral broadening is typically a combination of Kerr-induced self-phase modulation (SPM) and ionization-induced phase modulation due to plasma formation [5], which imparts a complicated spectral phase on the output of the S-HCF [6]. While chirped mirrors and fused silica compensate for GDD, compensating for higher order dispersion can be achieved by adding alternative material to the beam path. Ammonium dihydrogen phosphate (ADP), potassium dihydrogen phosphate (KDP), and water have been used for this purpose. [1].

Acousto-Optic Modulator (AOM)-based pulse-shapers (with the AOM placed in the Fourier plane of a zero dispersion stretcher) have proven to be powerful tools in the field of ultrafast spectroscopy, and are promising for implementing multidimensional spectroscopy techniques [7]. They function from the deep UV, across the visible, all the way to the mid-IR range [8,9]. They are also capable of pulse shaping on a shot-by-shot basis at repetition rates up to 100 kHz. While there are numerous examples of <10 fs pulses being generated using SLM and AOPDF pulse-shapers [10–12], pulse compression using a zero dispersion stretcher and AOM has remained limited to pulse durations greater than ~ 30 fs [13,14].

#440476 https://doi.org/10.1364/OSAC.440476
Journal © 2021 Received 24 Aug 2021; accepted 13 Oct 2021; published 7 Dec 2021

OSA CONTINUUM

The D-scan pulse characterization technique employed here consists of recording the second-harmonic (SHG) signal as a function of the quadratic spectral phase (chirp) of the pulse. This measurement technique is especially powerful because it combines pulse compression with characterization in a simple in-line setup. Additionally, the orders of the spectral phase (i.e. GDD, TOD, FOD, and 5th order) result in unique features in the spectrogram, which can be qualitatively interpreted without a reconstruction algorithm [15].

We report on the development of a stretched hollow-core fiber (S-HCF) apparatus, which utilizes either a novel motorized variable-thickness water cell or an AOM-based pulse-shaper to combine pulse compression, TOD compensation, pulse shaping and D-scan pulse characterization. We demonstrate compression down to durations around 5.5 fs. To the best of our knowledge, these are the shortest duration pulses from an AOM-based pulse-shaper, and the apparatus is currently being used for molecular coherent control experiments.

2. Apparatus

Figure 1 shows a schematic diagram of the stretched hollow-core fiber (S-HCF), pulse compression elements, and measurement apparatus. A Ti:Sa laser (1 kHz repetition rate, 1 W average power, 30 fs pulse duration, 780 nm center wavelength) injects pulses with energy up to 1 mJ into the S-HCF. The beam is focused by a 1 m lens to a 135 μm waist ($1/e^2$ intensity radius). This is close to the theoretically ideal value of 145 μm for this diameter fiber using the mode matching condition $w = 0.64a$, where $a = 225$ μm is the inner radius of the fiber [16]. The input (and output) beams are turned 90 degrees inside the vacuum chamber. The S-HCF (Molex 1068150625) has a 450 μm inner diameter, and is 2.1 m long (limited by the length of the optics table). Connectorizing the fiber consists of inserting it into a custom designed fiber connector, which is mounted in a fixture. Then epoxy (low viscosity Torr Seal) is injected into the connector through a hole which is cross-drilled relative to the one into which the fiber is inserted. Once the epoxy is cured the excess fiber is scored with a ruby scribe and cleaved. The connectorized fiber is mounted to bellows, which mate the S-HCF to the vacuum system, and are supported by kinematic mounts. The input to the HCF has 4 degrees of freedom, translation in x and y, and pitch and yaw. The output of the fiber has 5 degrees of freedom with the addition of translation in z, which allows tension to be applied to the fiber. Fiber tension is applied via the the micrometer on the z-axis translation stage. The mechanical rigidity of the kinematic mounts is sufficient to withstand pressures from 20 mTorr to about 1500 Torr, and with additional bracing (and smaller diameter entrance and exit windows) the apparatus has been successfully tested up to 3000 Torr.

The output of the S-HCF is collimated with a 875 mm focal length, curved, silver mirror. The variable-thickness water cell and chirped mirrors (Layertec 111346, -40fs^2 per double bounce), or pulse-shaper and 31 mm of BK7, are used in combination to provide the necessary dispersion control. Water has several advantages over fused-silica wedges, which are traditionally used as the bulk material for pulse compression. The dispersion of water is better suited for compressing the broadband pulses from HCFs because its TOD/GDD ratio is > 1 fs [5,17], which enables compensating residual negative TOD. Another advantage of a variable-thickness water cell is the long scan range. The water cell can scan from 1 mm to 2 cm and is limited only by the travel of the translation stage. The design of the variable-thickness water cell is conceptually simple. It consists of two windows and a bellows between them. One of the windows is mounted to a translation stage. We used 100 μm thick fused silica (microscope cover slides) for windows which are not AR coated, and the measured transmission through the cell is 82%. The clear aperture of the water cell is 9 mm, which allows transmission of the collimated output beam from the S-HCF. This water cell is placed before the chirped mirrors, where the pulse duration is relatively long, in order to prevent self-phase modulation and self-focusing from occurring inside the water cell. We observed no evidence of self-phase modulation at pulse energies up to 200 μJ through the cell.

OSA CONTINUUM

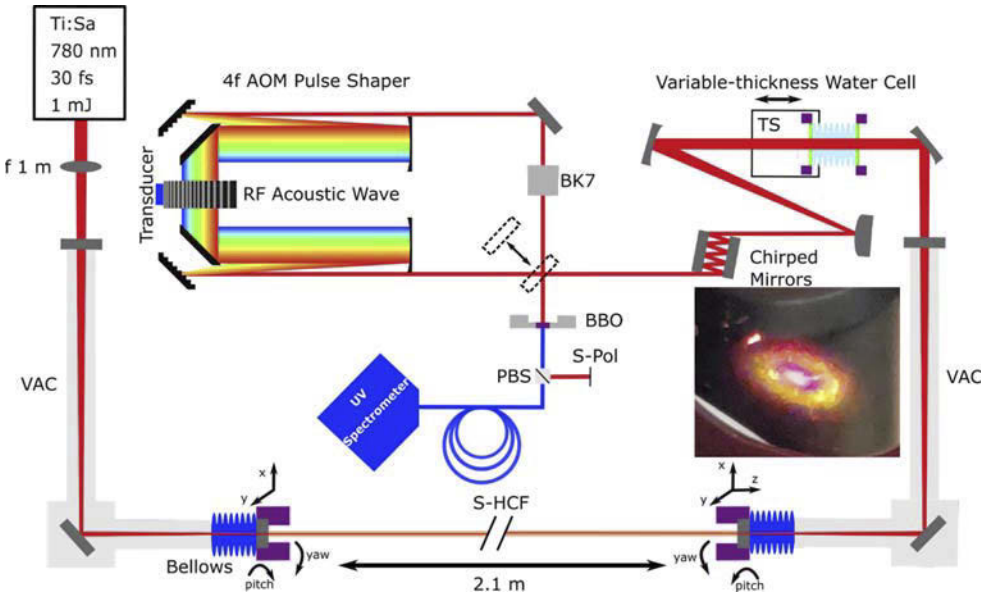

Fig. 1. Schematic diagram of the vacuum system (VAC), stretched hollow-core (S-HCF) fiber, pulse compression scheme and measurement apparatus. The broadband pulses are compressed using a combination of chirped mirrors and variable-thickness water cell actuated via a motorized translation stage (TS), or 4f AOM pulse-shaper and 31 mm of BK7 material. Characterization is performed via D-scan. The second harmonic is separated from the fundamental using a polarizing beam splitter (PBS) cube. The inset shows the spatial mode from the S-HCF, which was photographed off the face of a silver mirror.

The pulse-shaper is a 4f design where the shaping is performed in the frequency domain by placing a fused quartz AOM in the Fourier plane of a zero dispersion stretcher. As noted in earlier work, the nonlinear mapping of optical frequency to position in the AOM (due to the nearly linear variation in angle with λ from the diffraction grating and the inverse relationship between λ and ω) leads to a significant amount of higher-order dispersion. Following [13], the first three terms in the Taylor expansion after the constant and linear terms were calculated to be GDD=±2075 fs^2, TOD=∓4301 fs^3 FOD=±14860 fs^4, where the signs are to be read across. The emphasis is that these terms can either be positive or negative in overall sign. The orientation of the AOM (transducer toward the red/blue side of the optical spectrum) and its diffraction order (±1) control the sign of this phase, and with the appropriate choice (transducer toward the red side of the optical spectrum and +1 diffraction order or transducer toward the blue side of the optical spectrum and −1 diffraction order), the pulse-shaper can produce negative GDD for an unshaped acoustic wave, compensating for positive GDD associated with material dispersion (of windows, the AOM crystal etc). This allows for compression of the pulses without chirped mirrors, facilitates compensating for the remaining pulse-shaper dispersion by adding more normally dispersive material (e.g. fused silica or BK7) to the beam path, and prevents the pulse shaper from running out of RF bandwidth (which in this configuration allows for approximately ±1000fs^2 and ±2000fs^3 second and third order dispersion). We note that for +1 diffraction order with the transducer toward the blue side of the optical spectrum or −1 diffraction order and the transducer toward the red side of the optical spectrum, the pulse-shaper produces positive GDD for an unshaped acoustic wave.

We chose to place the transducer near the blue side of the optical spectrum in order to optimize the shape of the diffracted optical spectrum, since there is variation in diffraction efficiency

OSA CONTINUUM

with distance from the transducer and with acoustic wave frequency. For a chirped acoustic wave, this results in a diffraction efficiency variation with optical frequency, and changes to the spectrum are minimized for this configuration. Previous reports [13] of the AOM pulse compression also include Bragg angle correction. We explored this and found that it did not significantly improve the spectrum of the shaped pulses, whereas it did place an extra constraint on the shaped acoustic wave. Therefore, we focused on compensating for the nonlinear mapping between optical frequency and position on the AOM.

The pulse duration was measured by varying the dispersion of the pulse, using the water cell or the pulse-shaper, while recording the second harmonic generation signal in a 10 μm thick BBO crystal. We observed that the measured D-scan trace had sensitivity to the angle tuning of the BBO, indicating that the phase matching bandwidth of the 10 μm thick crystal, while adequate, is not ideal for our broad bandwidth. Understanding that the phase matching bandwidth was a factor, we experimented with angle tuning the BBO crystal, and were successful in balancing the red and blue components of the second harmonic spectra. Also, we note that one can still attain information on the phase of a particular frequency component, even if the second harmonic is not measured, as long as one can measure non-degenerate sum frequency generation with other frequency components [18]. A polarizing beamsplitter cube was used to filter out the fundamental from the second harmonic. While the PBS potentially limits our ability to measure UV in the SHG, measurements we performed with and without the PBS did not show a significant difference in the amount of signal below 300 nm. The D-scans were reconstructed using a custom phase retrieval algorithm. We used MATLAB's stochastic solver Particle Swarm to infer the phase of each constituent frequency in the fundamental spectrum by minimizing the sum of the squared difference between the measured and theoretical scans. The theoretical D-scans were calculated according to the formulas in [19,20].

Included in Fig. 1 is a picture of the beam mode from the S-HCF, which was taken off the face of a 1 inch silver mirror. A central bright spot and ring are visible. We observed this mode when the argon pressure in the fiber is increased above a few hundred mTorr. This phenomena is not observed when the argon gas is replaced with helium (or under vacuum) which suggests there is some self-focusing at the entrance of the fiber. A similar explanation for the mode appearing as a bright core with a large concentric ring is offered in [5]. We observed that if the ring is well-centered around the central bright spot then the mode and the spectrum output by the S-HCF are stable. This stability can be assured by fine-tuning the alignment of the laser into the fiber at low power.

3. Results

The S-HCF apparatus was pumped with 30 fs pulses, 352 mW average power (324 mW at the entrance of the fiber), and focused to 135 μm spot size. The S-HCF was statically filled with 1070 torr of argon. The usable power out of the S-HCF apparatus was 210 mW, and correcting for loses in the optics the calculated fiber transmission was 73%. Figure 2 shows a comparison between a) water D-scan, b) pulse-shaper D-scan, and c) pulse-shaper collinear frequency resolved optical gating (CFROG) [21]. The experimentally measured spectrograms (column 1) are consistent with their reconstructions (column 2). The time domain and minimum pulse durations, calculated from the reconstructions, are consistent between all three measurement techniques d) and are all on the order of 5 fs. The fundamental spectrum for the water D-scan and pulse-shaper D-scan are similar and span an octave of bandwidth e). The difference between the two fundamentals is attributed to the measurements being taken on different days.

For the water cell D-scans, the motorized water cell was translated 10 mm and the SHG spectrum was recorded for 101 steps. Modulations in the water D-scan spectrogram are likely caused by the chirped mirrors being not exactly at the ideal angle to cancel out the phase oscillations, and it has been documented that eliminating these spectral oscillations requires fine

OSA CONTINUUM

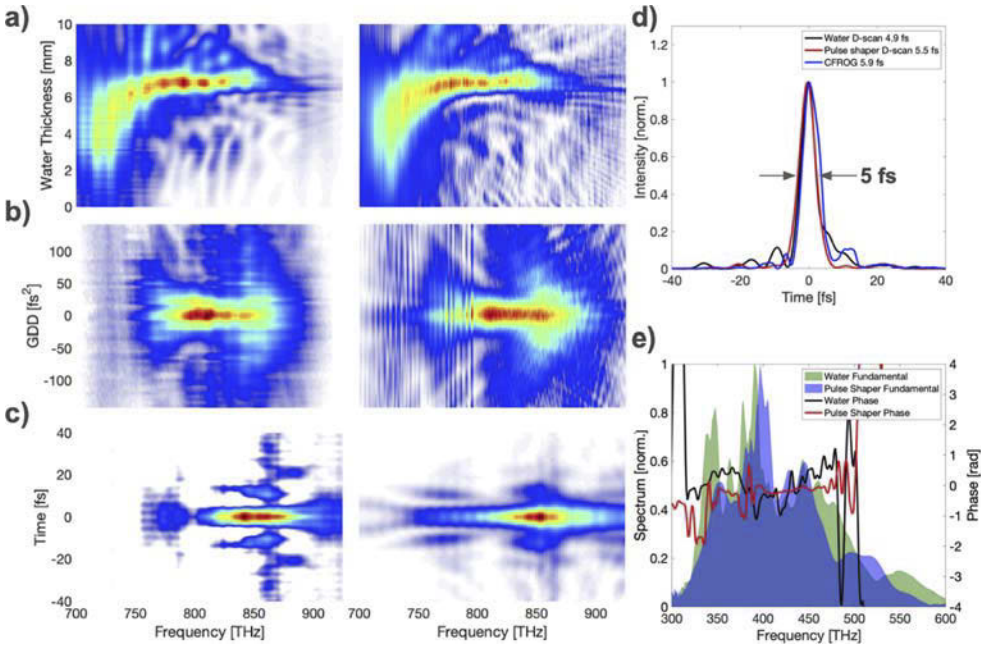

Fig. 2. Comparison of a) water cell D-scan, b) pulse-shaper D-scan, and c) pulse-shaper CFROG. The experimentally measured spectrograms (column 1) show good agreement with their reconstructions (column 2) and the reconstructed pulse durations d) are consistent with one another and are within ~1 fs of transform limit. The pulse durations are 4.9, 5.5, and 5.9 fs, respectively. e) shows the fundamental spectrum for the water D-scan and the pulse-shaper D-scan, and retrieved spectral phase for each of the measurements.

tuning of the chirped mirror angle [17]. The concave down curvature of the trace suggests residual fourth-order dispersion. The reconstructed pulse duration is 4.9 fs and the fundamental transform limit is 3.8 fs. The reconstruction error is <1%. The difference between the reconstructed pulse duration and the transform limit is not clear, although replacing the SHG crystal with a 5μm thick crystal may help.

For the pulse-shaper D-scan, the water cell and the chirped mirrors were removed. Bulk BK7 material was added to the beam path in order to compensate for the dispersion of the unshaped acoustic wave of the pulse-shaper. The choice of AOM configuration resulted in the leading term in the phase accrued as a result of the non-linear mapping between optical frequency to AOM position being equal to -2075 fs^2. This was compensated for by using 31 mm of BK7 (GVD=48.3 fs$^2/mm$ @ λ_0 = 763 nm, GDD=1496 fs^2). With the addition of the 10 mm fused silica AOM crystal (GDD=392 fs^2), the GDD sums to 1888 fs^2—which almost completely compensates for the -2075 fs^2 imparted by the unshaped acoustic wave of the pulse-shaper. The cancellation of the GDD reserves the pulse-shaper's RF bandwidth for higher order phase correction, which is a critical factor when shaping octave-spanning bandwidths.

The fundamental for the pulse-shaper D-scan (Fig. 2(e)) is slightly different from the fundamental for the water D-scan and contains less IR light. By using the phase compensation technique discussed above, the pulse-shaper RF bandwidth remained within 3dB limits of the AOM [100, 200] MHz across the majority of the optical bandwidth, except for approximately ν>570 THz. As a result, the fundamental before the pulse-shaper was consistent with the diffracted fundamental while pulse shaping. The power out of the pulse-shaper was 15 mW, corresponding to a transmission efficiency of 11%.

OSA CONTINUUM

In order to obtain the D-scans presented in panel b) of Fig. 2, we first scanned the GDD from -500 fs^2 to $+500$ fs^2 while applying the calculated TOD and FOD necessary to correct for the unshaped acoustic wave (TOD=-4301 fs^3 FOD=14860 fs^4). The D-scan trace was then reconstructed and the retrieved phase (i.e. the residual spectral phase at the point of minimum pulse duration - panel e) of Fig. 2) was inverted and programmed back into the pulse-shaper. Some iteration of this procedure was required since the D-scan inversion algorithm produced some errors for scans where the minimum pulse duration is significantly larger than the transform limit. The final measured D-scan is in good agreement with the reconstruction (Fig. 2(b)) and yields a minimum pulse duration of 5.5 fs (4.6 fs transform limit) (Fig. 2(d)). A notable feature is the lack of IR in the pulse-shaper D-scan measurement compared to the water D-scan, which is consistent with less IR observed in the pulse-shaper fundamental.

Row c) shows a pulse-shaper CFROG measurement [21] and reconstruction [22], and the fact that this reconstruction is consistent with the D-scans offers validation of the pulse characterization as well as the D-scan technique. The fundamental spectrum for the CFROG measurement is the same as the water D-scan, and the reconstructed pulse duration is 5.9 fs. The FROG retrieval algorithm used a 1024 grid and reported an error of $<1\%$. The benefit of the collinear FROG is that the scan is performed by using the pulse shaper to create the pulse pairs and control the delay. This has the advantage of eliminating the difficulty of setting up a Mach Zehnder interferometer for such short pulses where minor alignment issues could lead to temporal smearing in the SHG crystal, thus recording artificially longer pulses. A standard FROG retrieval algorithm was used to reconstruct the pulse. As discussed in [21] we were able to Fourier Filter the CFROG signal to recover a standard FROG trace.

A notable feature is that essentially no second harmonic is observed in the measured D-scans at frequencies greater than 900 THz, despite the fact that both fundamentals contain light at frequencies greater than 450 THz. This is likely due to the limited phase matching bandwidth of the BBO crystal combined with the response of the UV spectrometer and associated optics. Since, the phenomena is observed for the water D-scan as well as the pulse-shaper D-scan it is not related to the AOM running out of RF bandwidth in the blue range of optical frequencies. The reconstruction algorithm deals with this problem by adding an abnormal phase to the blue side of the spectrum, which can be seen in the phase plots in panel e) of Fig. 2.

We also experimented with a shorter 1.3 m fiber, compared to the 2.1 m long fiber results we report on in this work. We have observed that the spectrum from the 1.3 m fiber is comparable to the spectrum from a 2.1 m fiber if the gas pressure or laser pulse intensity is increased for the shorter fiber. However, if the comparison is made for the same intensity and gas pressure, then the longer fiber produces a broader spectrum, but not proportional to the increase in path length. Thus we suspect that extending the length of the 2.1 m fiber might produce a modest increase in the broadening at comparable pressures and laser intensities. Finally, the pulse shaper was also used to modify the spectral amplitudes which allows for arbitrary pulse shapes (see Supplement 1).

4. Conclusion

We demonstrate spectral phase control of broadband pulses from a home built stretched hollow-core fiber apparatus by compressing them to nearly transform limit using a variable-thickness water cell, and an AOM-based 4f pulse-shaper. Measurements of the pulse duration obtained by water D-scan, pulse-shaper D-scan, and CFROG yielded consistent < 6 fs results. These shaped octave-spanning pulses are now being used for time-resolved (pump-probe) measurements of excited state molecular dynamics, and can be focused to intensities sufficient for strong field molecular ionization. The ability to generate intense, ~5 fs pulse pairs with the pulse-shaper enables pump probe measurements with phase locked pulses and arbitrary (delay dependent) relative amplitude [23]. It also enables measurements with shaped laser fields that can be used

OSA CONTINUUM

to interrogate and control double ionization [24–26], high harmonic generation [27], angular streaking [28], and nonadiabatic dynamics in strong field ionization [29].

Funding. National Science Foundation (1806294).

Acknowledgements. We gratefully acknowledge technical discussions with Ruaridh Forbes and support from the National Science Foundation under award number 1806294.

Disclosures. The authors declare no conflicts of interest.

Data availability. Data underlying the results presented in this paper are not publicly available at this time but may be obtained from the authors upon reasonable request.

Supplemental document. See Supplement 1 for supporting content.

References

1. H. Timmers, Y. Kobayashi, K. F. Chang, M. Reduzzi, D. M. Neumark, and S. R. Leone, "Generating high-contrast, near single-cycle waveforms with third-order dispersion compensation," Opt. Lett. **42**(4), 811–814 (2017).
2. M. Nisoli, S. De Silvestri, and O. Svelto, "Generation of high energy 10 fs pulses by a new pulse compression technique," Appl. Phys. Lett. **68**(20), 2793–2795 (1996).
3. T. Nagy, M. Forster, and P. Simon, "Flexible hollow fiber for pulse compressors," Appl. Opt. **47**(18), 3264–3268 (2008).
4. M. Miranda, C. L. Arnold, T. Fordell, F. Silva, B. Alonso, R. Weigand, A. L'Huillier, and H. Crespo, "Characterization of broadband few-cycle laser pulses with the d-scan technique," Opt. Express **20**(17), 18732–18743 (2012).
5. T. Nagy, M. Kretschmar, M. J. Vrakking, and A. Rouzée, "Generation of above-terawatt 1.5-cycle visible pulses at 1 khz by post-compression in a hollow fiber," Opt. Lett. **45**(12), 3313–3316 (2020).
6. P. Hölzer, W. Chang, J. Travers, A. Nazarkin, J. Nold, N. Joly, M. F. Saleh, F. Biancalana, and P. S. J. Russell, "Femtosecond nonlinear fiber optics in the ionization regime," Phys. Rev. Lett. **107**(20), 203901 (2011).
7. S.-H. Shim and M. T. Zanni, "How to turn your pump–probe instrument into a multidimensional spectrometer: 2d ir and vis spectroscopies via pulse shaping," Phys. Chem. Chem. Phys. **11**(5), 748–761 (2009).
8. S.-H. Shim, D. B. Strasfeld, and M. T. Zanni, "Generation and characterization of phase and amplitude shaped femtosecond mid-ir pulses," Opt. Express **14**(26), 13120–13130 (2006).
9. F. Nicolai, N. Müller, C. Manzoni, G. Cerullo, and T. Buckup, "Acousto-optic modulator based dispersion scan for phase characterization and shaping of femtosecond mid-infrared pulses," Opt. Express **29**(13), 20970–20980 (2021).
10. E. Matsubara, K. Yamane, T. Sekikawa, and M. Yamashita, "Generation of 2.6 fs optical pulses using induced-phase modulation in a gas-filled hollow fiber," J. Opt. Soc. Am. B **24**(4), 985–989 (2007).
11. N. Karasawa, L. Li, A. Suguro, H. Shigekawa, R. Morita, and M. Yamashita, "Optical pulse compression to 5.0 fs by use of only a spatial light modulator for phase compensation," J. Opt. Soc. Am. B **18**(11), 1742–1746 (2001).
12. V. Loriot, G. Gitzinger, and N. Forget, "Self-referenced characterization of femtosecond laser pulses by chirp scan," Opt. Express **21**(21), 24879–24893 (2013).
13. A. C. Jones, M. B. Kunz, I. Tigges-Green, and M. T. Zanni, "Dual spectral phase and diffraction angle compensation of a broadband aom 4-f pulse-shaper for ultrafast spectroscopy," Opt. Express **27**(26), 37236–37247 (2019).
14. M. R. Fetterman, D. Goswami, D. Keusters, W. Yang, J.-K. Rhee, and W. S. Warren, "Ultrafast pulse shaping: amplification and characterization," Opt. Express **3**(10), 366–375 (1998).
15. I. Sytcevich, C. Guo, S. Mikaelsson, J. Vogelsang, A.-L. Viotti, B. Alonso, R. Romero, P. T. Guerreiro, Í. J. Sola, A. L'Huillier, and H. Crespo, "Characterizing ultrashort laser pulses with second harmonic dispersion scans," J. Opt. Soc. Am. B **38**(5), 1546–1555 (2021).
16. R. Abrams, "Coupling losses in hollow waveguide laser resonators," IEEE J. Quantum Electron. **8**(11), 838–843 (1972).
17. F. Silva, M. Miranda, B. Alonso, J. Rauschenberger, V. Pervak, and H. Crespo, "Simultaneous compression, characterization and phase stabilization of gw-level 1.4 cycle vis-nir femtosecond pulses using a single dispersion-scan setup," Opt. Express **22**(9), 10181–10191 (2014).
18. B. Alonso, Í. J. Sola, and H. Crespo, "Self-calibrating d-scan: Measuring ultrashort laser pulses on-target using an arbitrary pulse compressor," Sci. Rep. **8**(1), 3264 (2018).
19. E. Escoto, A. Tajalli, T. Nagy, and G. Steinmeyer, "Advanced phase retrieval for dispersion scan: a comparative study," J. Opt. Soc. Am. B **35**(1), 8–19 (2018).
20. M. Miranda, J. Penedones, C. Guo, A. Harth, M. Louisy, L. Neoričić, A. L'Huillier, and C. L. Arnold, "Fast iterative retrieval algorithm for ultrashort pulse characterization using dispersion scans," J. Opt. Soc. Am. B **34**(1), 190–197 (2017).
21. I. Amat-Roldán, I. G. Cormack, P. Loza-Alvarez, E. J. Gualda, and D. Artigas, "Ultrashort pulse characterisation with shg collinear-frog," Opt. Express **12**(6), 1169–1178 (2004).
22. R. Trebino, K. W. DeLong, D. N. Fittinghoff, J. N. Sweetser, M. A. Krumbügel, B. A. Richman, and D. J. Kane, "Measuring ultrashort laser pulses in the time-frequency domain using frequency-resolved optical gating," Rev. Sci. Instrum. **68**(9), 3277–3295 (1997).

OSA CONTINUUM

23. V. Tagliamonti, B. Kaufman, A. Zhao, T. Rozgonyi, P. Marquetand, and T. Weinacht, "Time-resolved measurement of internal conversion dynamics in strong-field molecular ionization," Phys. Rev. A **96**(2), 021401 (2017).
24. C. Cheng, Z. L. Streeter, A. J. Howard, M. Spanner, R. R. Lucchese, C. W. McCurdy, T. Weinacht, P. H. Bucksbaum, and R. Forbes, "Strong field ionization of water ii: Electronic and nuclear dynamics en route to double ionization," arXiv preprint arXiv:2104.05869 (2021).
25. M. Kübel, K. Betsch, N. G. Kling, A. Alnaser, J. Schmidt, U. Kleineberg, Y. Deng, I. Ben-Itzhak, G. Paulus, T. Pfeifer, and J. Ullrich, "Non-sequential double ionization of ar: from the single-to the many-cycle regime," New J. Phys. **16**(3), 033008 (2014).
26. Z. Chen, F. Liu, H. Wen, T. Morishita, O. Zatsarinny, and K. Bartschat, "Nonsequential double ionization of ar in near-single-cycle laser pulses," Opt. Express **28**(15), 22231–22246 (2020).
27. J. Schötz, B. Förg, W. Schweinberger, I. Liontos, H. Masood, A. Kamal, C. Jakubeit, N. Kling, T. Paasch-Colberg, S. Biswas, and M. Högner, "Phase-matching for generation of isolated attosecond xuv and soft-x-ray pulses with few-cycle drivers," Phys. Rev. X **10**(4), 041011 (2020).
28. M. Kübel, Z. Dube, A. Y. Naumov, M. Spanner, G. G. Paulus, M. F. Kling, D. M. Villeneuve, P. B. Corkum, and A. Staudte, "Streak camera for strong-field ionization," Phys. Rev. Lett. **119**(18), 183201 (2017).
29. V. Tagliamonti, P. Sándor, A. Zhao, T. Rozgonyi, P. Marquetand, and T. Weinacht, "Nonadiabatic dynamics and multiphoton resonances in strong-field molecular ionization with few-cycle laser pulses," Phys. Rev. A **93**(5), 051401 (2016).